Biometrical Letters
Vol. 43 (2006), No. 1, 49-66

Some considerations on the use of geostatistical methods in agricultural field trials Part I: From point to regularized data - theoretical considerations

Christel Richter*, Bärbel Kroschewski

Department of Biometry and Experimental Design, Humboldt-Universität zu Berlin, Faculty of Agriculture and Horticulture, 10115 Berlin, Invalidenstraße 42, Germany;

SUMMARY

Over the last years, agricultural experimenters have shown increased interest in geostatistical methods. Geostatistical methods provide the opportunity to take into account spatial dependencies between plots in experiments. The spherical or the exponential model is often used to describe the dependence. Originally, however, these models were developed however, for point data. In agricultural field experiments, the data mostly result from transects or plots which are laid out on grids in the x-y plane. Transect or plot data arise by regularization of point data. Assuming the spherical and the exponential model (with isotropy and anisotropy, with and without nugget) as the initial models, we investigate the covariogram functions and their characteristic parameters for different regularizations in part I of this paper. Because explicit expressions for the resulting covariance functions can be specified only as an exception, we made use of simulations. The calculations were performed in both the x- and y-directions as well as omnidirectionally. Except for isotropic initial covariograms and quadratic plots, the regularized covariograms show anisotropy in all cases and are generally characterized by a sigmoid shape. In the second part of this paper which will appear in the next issue of the *Biometrical Letters*, the theoretical results will be confronted with those from uniformity trials.

Key words: geostatistical methods, point data, regularized data, agricultural field trials

*Corresponding author. D-10115 Berlin, Invalidenstraße 42, phone: +49 30 2093 8483; fax: +49 30 2093 8460, e-mail: ch.richter@agrar.hu-berlin.de

1. Introduction

It is generally accepted that covariances exist in agricultural field experiments between neighbouring plots. Covariances arise from the competition of plants for above-ground and below-ground resources on the one hand, and from similar soil and other environmental effects of adjacent plots on the other hand. As to the grain yield, Wiebe (1935) has already pointed to the existence of positive, decreasing with increasing distance, correlations between plots. The principle of randomization is the classic approach taken in order to overcome ("to neutralize" –Zimmerman and Harville, 1991) correlated errors (Yates (1938)). In conjunction with the arrangement in blocks (Fisher, 1935), it is the most established method in field experiments to date. In the standard linear model, these two basic principles (randomization and blocking) result in uncorrelated observations (fixed blocks) or observations with constant correlations (random blocks) within blocks. The positive effects of blocking and randomization (unbiased estimates of treatment differences and reduced error variability) depend on a correct assessment of soil heterogeneity.

At the same time other concepts for considering spatial dependence were pursued - the so-called nearest-neighbour methods. They were presented by Papadakis (1937) and Bartlett (1938). These methods were primarily developed heuristically. They used residuals of neighbouring plots as 'covariates' to allow for local fertility effects.

At the end of the sixties, doubts arose as to whether the necessary information for the proper layout of experiments in blocks is given in all cases, and the question came up of how to handle misjudgements of heterogeneity. This led to a renewal of the ideas of Papadakis and Bartlett. The statistical background was elaborated by trying to overcome some statistical deficits of the original method and of derived concepts. However, none of the concepts became accepted as a common school of thought for the analysis of experiments.

Geostatistical methods might be another approach to overcoming the problem described. In recent years they have gained the interest of agricultural experimenters. Whereas the nearest- neighbour methods indirectly take spatial effects into account, the geostatistical methods model the spatial dependence directly. The geostatistical approach has been discussed by several authors, e.g. to analyze uniformity trials (Zimmerman and Harville, 1991), regarding its use in the planning phase (Ersbøll, 1996) as well as in the analysis of accomplished designed experiments with many treatments (Brownie et al., 1993; Stroup et al., 1994; Littell et al., 1996; Stroup, 2002).

The philosophical background of the different schools of thought for data modelling of field experiments is discussed by Schabenberger and Pierce (2002). It can be expected that discussion of the advantages and disadvantages of the

different approaches will intensify over the course of the next years. With the mixed model theory and the corresponding software implementation, important preconditions are met for a broader use of geostatistical methods for designed experiments.

The mathematical tool used to describe the dependence or independence of regionalized data is the covariance or the semivariance function. In case of second order stationarity, both functions are equivalent instruments. While in original geostatistical applications - problems of evaluating mining deposits - it is often sufficient to assume the intrinsic hypothesis, we will focus on the covariance function, i.e. we assume second order stationarity, since in conjunction with mixed model theory the estimation of covariances is at the centre of attention.

The often-used covariance or semivariance models – the spherical and exponential model with and without nugget - are originally those for point data. The term *point data* means that they have a punctual support. A punctual support (infinitely small support) is only an idealization that does not exist in reality; it is obviously a relative term. Data which come from a higher-dimensional support - one dimension (core, transect), two dimensions (plot, block) or three dimensions (volume) - are called *regularized data*. In field experiments, as well as in mining, one is often interested in semivariance / covariance functions for regularized data. In mining geostatistics, it is well known that the regularization changes the characteristics of the semivariance functions. Many authors deal with this problem. In contrast, one finds in the literature about geostatistics in agricultural field experiments that the spherical or exponential model is often used for data from higher dimensional supports. The question is whether these simple models provide a really sufficient fit in this field or rather if the effect of regularization should be taken into account.

In this paper we will focus on the relations between the covariograms of point and regularized data. By way of an example, we consider the spherical and exponential model for point data. The known results of mining geostatistics will be used. Moreover, the special layout of agricultural experiments and the possible omnidirectional calculation will be taken into account.

In the following we denote the point data by P or 1x1, transect data by 1xL or Lx1 and plot data by axb.

Let $Cov_P(h)$ be the covariance function of point data and $Corr_P(h)$ the corresponding correlation function. For the isotropic spherical model with nugget variance, $Cov_P(h)$ is

$$Cov_P(h) = \begin{cases} C_0 + C & \text{if } h = 0 \\ C \cdot \left[1 - \frac{3}{2} \cdot \frac{h}{A} + \frac{1}{2} \cdot \left(\frac{h}{A} \right)^3 \right] & 0 < h \le A \\ 0 & \text{if } h > A \end{cases}$$

and for the isotropic exponential model with nugget variance:

$$Cov_P(h) = \begin{cases} C_0 + C & \text{if } h = 0 \\ C \cdot e^{\frac{-h}{A^*}} & \text{if } h > 0 \end{cases} \tag{2}$$

with h distance, C_0 nugget variance, C partial sill, C_0 + C sill, A range and A* range parameter.

The correlation function $Corr_P(h)$ is equal to $Cov_P(h)/(C_0+C)$ for each model.

For $h \approx 3 \cdot A^*$ the covariance of the exponential model is equal to $0.05 \cdot C$. This distance is often denoted as the practical range of the exponential model. In case of an existing nugget, it seems reasonable to denote that distance as the practical range, where $Corr_P(h) = 0.05$. This is fulfilled for $h = -A^* \cdot \log\{0.05(1 + C_0/C)\}$. Both distances are equal in the case of no nugget. The quotient $0 \le C_0/(C_0+C) \le 1$ gives the proportion of spatial structure *PSS*.

2. Introductory example and derived problems

At first, we will consider the one-dimensional extension of the support. In mining, two forms of this regularization are observed: regularization by samples within a core and the regularization over constant thickness (Rendu, 1981). In Figure 1, the two forms are illustrated in the x-y plane. The analysis of cores in mining corresponds to that of transects in agricultural applications.

The transects may have length L. If they are oriented in the y-direction (as in Fig. 1), we use the abbreviation 1xL, for the orientation in the x-direction (parallel to the x-axis) we write Lx1.

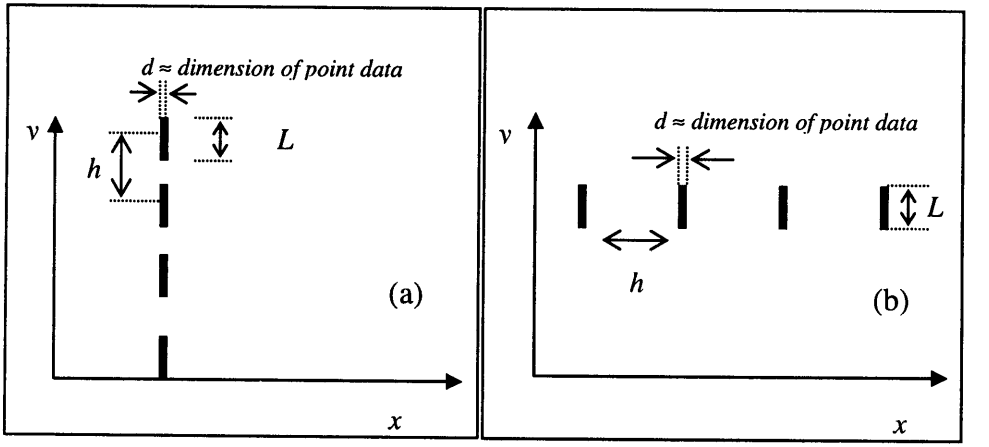

Fig. 1: Two forms of one-dimensional regularization in the xy-plane: regularization by samples within a core (a) and regularization over constant thickness (b).

Let $Corr_{1xL}(h)$ be the regularized correlation function for 1xL transects.

For demonstration we use the exponential model *without* nugget ($C_0 = 0$). In the y-direction (Fig. 1, a), $Corr_{1xL}(h)$ is the solution of the double integrals in (3):

$$Corr_{1xL}^{y\text{-}dir}(h) = \begin{cases} \frac{1}{L^2} \cdot \left[\int_0^h \int_h^{h+L} e^{\frac{-(y1-y)}{A^*}} dy1\, dy + \int_h^L \left\{ \int_h^y e^{\frac{-(y-y1)}{A^*}} dy1 + \int_y^{h+L} e^{\frac{-(y1-y)}{A^*}} dy1 \right\} dy \right] & \text{if } h \le L \\ \frac{1}{L^2} \cdot \int_0^L \int_h^{h+L} e^{\frac{-(y1-y)}{A^*}} dy1\, dy & \text{if } h > L \end{cases} \quad (3)$$

In this case an explicit solution is possible and is given in (4). Journel and Huijbregts (1978) have given the expression for the corresponding semivariogram.

$$Corr_{1xL}^{y\text{-}dir}(h) = \begin{cases} \frac{A^*}{L^2} \cdot \left[2L - 2h + A^* \cdot e^{\frac{-(h+L)}{A^*}} - 2A^* \cdot e^{\frac{-h}{A^*}} + A^* \cdot e^{\frac{h-L}{A^*}} \right] & \text{if } h \le L \\ \left(\frac{A^*}{L} \right)^2 \cdot \left[e^{\frac{L}{A^*}} + e^{\frac{-L}{A^*}} - 2 \right] \cdot e^{\frac{-h}{A^*}} & \text{if } h > L \end{cases} \quad (4)$$

In most situations, no analytical solution of the integrals exists and numerical integration is necessary. E.g. to get the solution for the isotropic case in the x-direction (Fig. 1, b), (5) must be numerically solved.

$$\mathrm{Corr}_{1xL}^{x\text{-}dir}(h) = \frac{2}{L^2} \cdot \int_0^L (L-u) \cdot e^{\frac{-\sqrt{h^2+u^2}}{A^*}} du \qquad (5)$$

For h = 0, the values of (4) and (5) are equal to (6) which is the mean correlation $\overline{\mathrm{Corr}}_{P\,in\,1xL}$ of the points in 1xL (cf. Rendu, 1981, for the standardized semivariogram).

$$\mathrm{Corr}_{1xL}(0) = \overline{\mathrm{Corr}}_{P\,in\,1xL} = 2\left(\frac{A^*}{L}\right)^2 \cdot \left[e^{\frac{-L}{A^*}} + \frac{L}{A^*} - 1\right] \qquad (6)$$

Figure 2 shows the exponential isotropic point correlogram for A* = 10 and C_0 = 0 as well as the corresponding regularized correlograms from (4) and (5) for 1xL = 1x15.

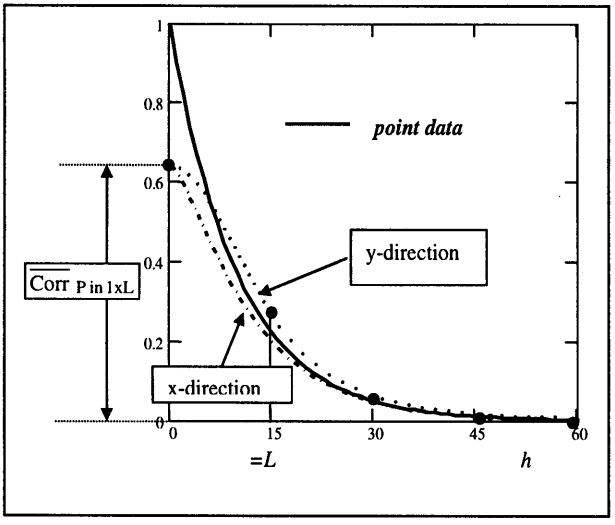

Fig. 2: Exponential isotropic correlograms for point data Corr_P (h) and for regularized data Corr_{1xL}(h) in two directions (A* = 10, C_0 = 0, 1xL = 1x15)

For a given h > 0, the correlations in the y-direction are larger than those for the x-direction. This can be illustrated as follows: Let h = L = 15. In the y-direction the midpoints of the two transects have the distance L, and the mean distance between all points of the first and the second transect is equal to L as

well (Fig. 1, a). In the x-direction all points of the first transect have only one point in the second transect with the distance L, for all other point pairs the distance is larger than L, so that the mean distance is larger than L (Fig. 1, b). Larger distances are followed by smaller correlations, so that the values in the y-direction are higher than those for the x-direction.
If the transects are assumed not to be overlapping, an empirical covariogram in the y-direction can only be calculated for h = 0, L, 2L, 3L.... (bold dots in Fig. 2). In this direction the practical range is approximately

$$\text{pract. range}_{1xL}^{y-dir} \approx 3 \cdot A^* + A^* \cdot \ln\left(\frac{A^{*2}}{L^2} \cdot \left[e^{\frac{L}{A^*}} + e^{\frac{-L}{A^*}} - 2\right]\right),$$

that is ≈ 31.8 in the example. In the x-direction with increasing L, the practical range decreases: from 29.96 (≈ 3A*) for the point data to 29.36 for L = 15 (by numerical integration of (5)).

In the y-direction a point of inflection can be noticed for $h = A^* \cdot \ln\sqrt{2e^{\frac{L}{A^*}} - 1}$ = 10.37 < L (i.e. in the non-observable region for non-overlapping transects) and in the x-direction for h ≈ 4.15 in the example.

The maximum difference between the two directional correlograms is a function of A* and L. We calculated the maximum over all distances h = 0, L, 2L, 3L... (observable distances in both directions) for different combinations of A* and L. In Figure 3 this maximum is represented for A* = 1...15 and L = 1...30. For L ≈ 1.8·A* the maximum differences are generally the largest and equal to 0.0694. In the example (A* =10, L = 15) the maximum is 0.068 (+ in figure 3) and it is achieved for h = L (Fig. 2).

For isotropic point data and transects oriented in the x-direction (Lx1), the above statements remain valid if the meaning of the x- and y-direction are exchanged. It follows especially from (6), that $Corr_{1xL}(0) = Corr_{Lx1}(0)$.

From Figure 2, (4), (5) and (6), the following conclusions can be drawn:

- the regularized covariogram/correlogram depends on the direction of regularization,
- the shape of the regularized model changes in relation to the point model (sigmoid shape).

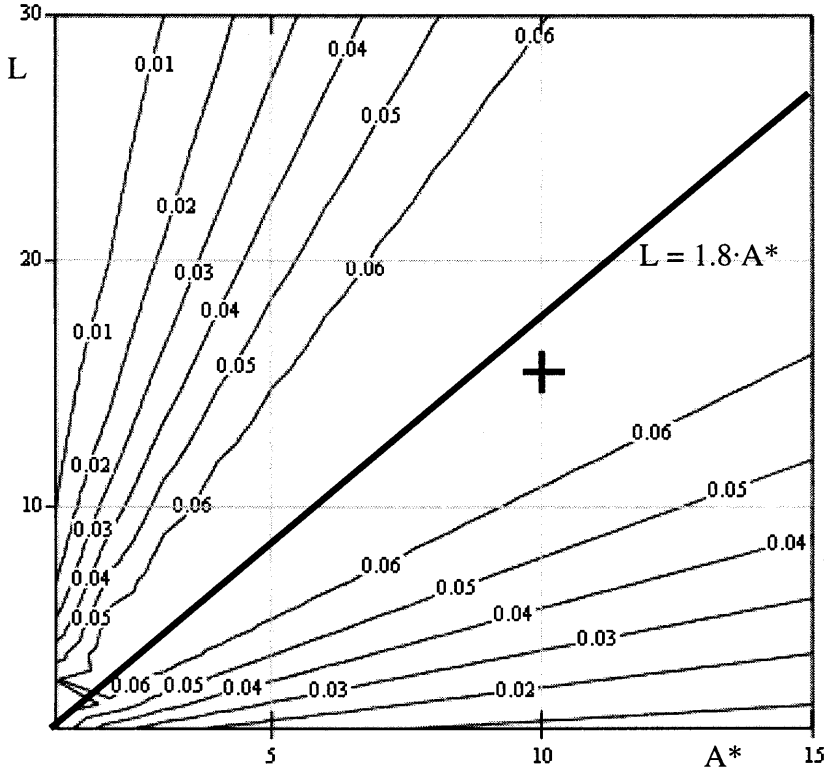

Fig. 3: Maximum differences between the two directional exponential isotropic correlograms as a function of A* and L. The sign + represents the discussed example with A* = 10 and L = 15.

In addition to the discussed layout of transects, a combination of (a) and (b) in Figure 1 is characteristic for agricultural applications. Moreover, the regularization in two dimensions (plots) is of special interest (Fig. 4). For such a layout, the calculation of covariograms is not only possible in the x- or y-direction with a hither to implicitly assumed tolerance angle of 0^0, but also in the x- and y-direction and other selected directions with different tolerance angles or over all directions (omnidirectional). The omnidirectional calculation is an analysis that is very often used.

Therefore, in the following, we will focus on two questions:

1. What are the characteristics of a transect covariogram, which is calculated omnidirectionally?
2. What holds for the omnidirectional covariogram of plots in relation to the directional ones (in x- and y-direction with tolerance angle 0^0)?

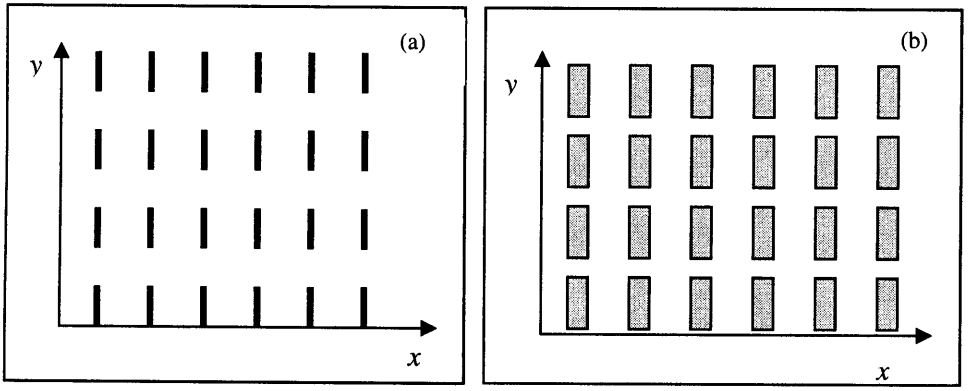

Fig. 4: Two forms of generalized regularized investigation: transects (a) and plots (b)

Due to the above mentioned difficulties in analytical integration (for plots, quadruple integrals must be considered) and to additional complications by an omnidirectional investigation, we approach the problem by means of simulations. With PROC SIM2D of SAS release 9.1.3, we simulated 14, 400, 000 data points for each of the variants in table 1 (1000 simulations on a grid 1x1 with dimension 120x120) and summarized them into transects and plots, which covered the whole grid and did not overlap. On the basis of the simulations, the 1xL-transect covariograms can then be calculated in x-direction for h = 0, 1...120 (we restricted ourselves to 60) and in y-direction for h = 0, L, 2L ... 120 and vice versa for Lx1-transects. For simulation defaults we chose some typical situations: with and without nugget, isotropy and anisotropy combined with the spherical or exponential model (table 1).

Table 1. Three simulation variants (1) to (3) with point data and one- and two-dimensional regularizations analyzed.

nugget + partial sill	**isotropy spherical A = 20**	**isotropy exponential A* = 10**	**geometric anisotropy exponential** $A^*_x = 10$ $A^*_y = 15$
	(1)	cf. introductory example	*(3)*
0 + 100	transects rectangular and quadratic plots	transects	transects in x- and y-direction
		(2)	
50 + 50	–	transects	–

3. Selected theoretical and simulation results

3.1 Transects - default (1) – no nugget, isotropy, spherical

For the default (1) from table 1 and different 1xL-transects, the omnidirectional covariograms are demonstrated in figure 5 (a). The initial isotropy of the point data results in an anisotropic omnidirectional covariogram for the transect data.

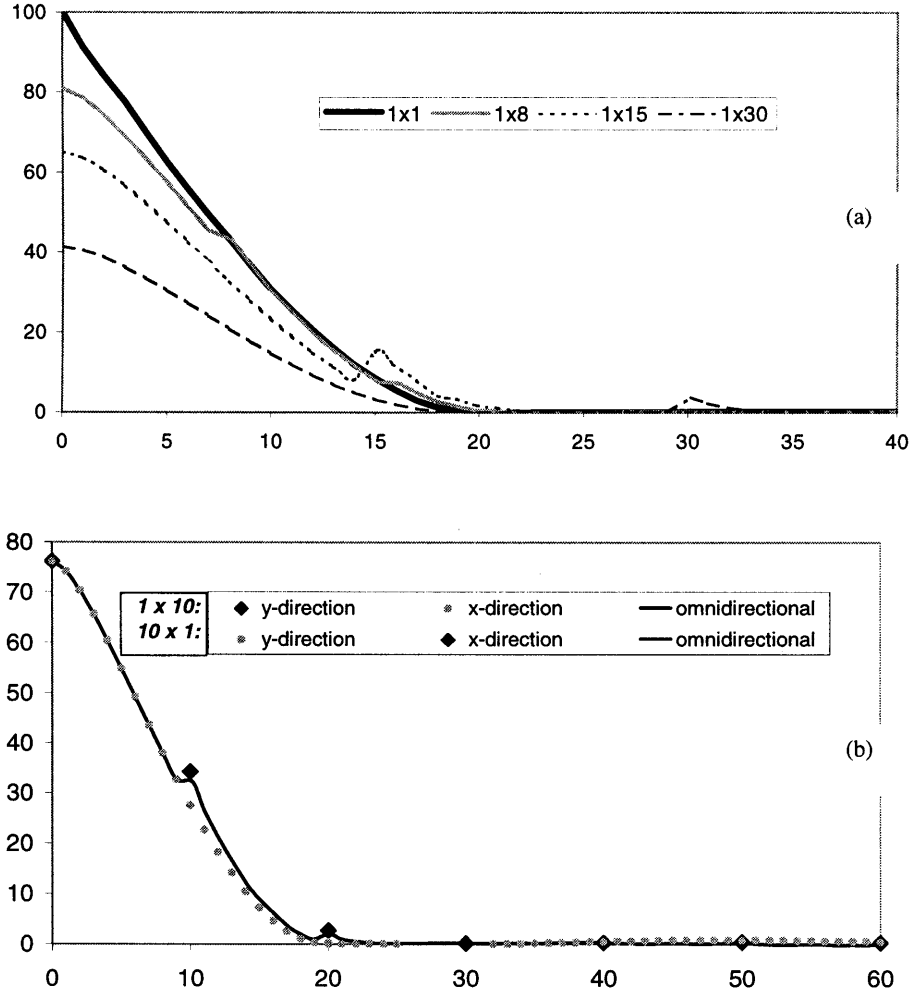

Fig. 5: Simulation default: isotropic, A = 20, C_0 = 0 and C = 100.
(a) Simulated omnidirectional spherical covariograms for point data (1x1) and for transect data.
(b) Omnidirectional as well as directional covariograms for 1x10 and 10x1.

Be $Cov_{1xL}(h)$ the regularized covariogram function of *any* model *without nugget*. The regularized sill is given in (7)

$$sill_{1xL} = \overline{Cov}_{P\,in\,1xL} = Cov_{1xL}(0) = C \cdot Corr_{1xL}(0) = sill_{point} \cdot \overline{Corr}_{Pin\,1xL} \qquad (7)$$

With increasing L, the correlation of the points in the transect is decreasing. Thus the sill of the regularized function becomes smaller the larger L is (c.p. figure 5).

In the spherical isotropic case, the mean covariance of the points in 1xL is

$$\overline{Cov}_{P\,in\,1xL} = \begin{cases} C\left[1 + \frac{1}{20} \cdot \left(\frac{L}{A}\right)^3 - \frac{L}{2A}\right] & L \le A \\ C\left[\frac{3}{4} \cdot \frac{A}{L} - \frac{1}{5}\left(\frac{A}{L}\right)^2\right] & L \ge A \end{cases} \qquad (8)$$

(c.p. Rendu, 1981, for the standardized semivariogram).

Because of isotropy, 1xL can be replaced by Lx1 in (7), (8) and in figure 5 (a).

It is remarkable that all graphs show jump discontinuities if h is an integral multiple of L. This is explained in figure 5 (b) for 1xL = 1x10. For $h < L = 10$, the omnidirectional covariogram is equal to the one in x-direction since for $h < L$ there is no transect in any other direction. Whenever the calculation in y-direction is possible (for h = 10 and 20), the function jumps to higher values because the covariance is higher in this direction (cp. fig. 2). For $h \ge 30$, all point pairs are independent. As a consequence, the range in y-direction is equal to A + L (= 30) whereas in x-direction it is A (= 20). In the interval $10 \le h < 30$, the omnidirectional covariogram lies between the two directional ones.

The maximum difference between the two directional correlograms, calculated over h = 0, L, 2L, 3L..., is achieved for h = L. In figure 6 the maximum is represented as dependent on A and L. For $L \approx 0.82 \cdot A$, the maximum differences are generally the largest and equal to 0.122.

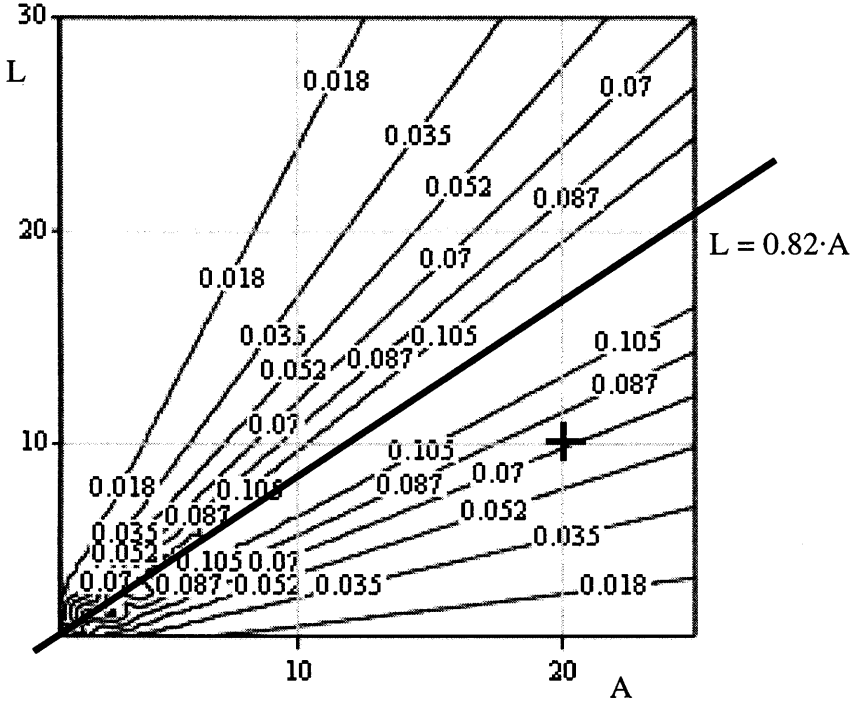

Fig. 6: Maximum differences between the two directional spherical isotropic correlograms as a function of A and L. + Example with A = 20 and L = 10 (Figure 5).

3.2 Transects - default (2) – nugget, isotropy, exponential

For default (2) from table 1 as well as for different transect lengths, the omnidirectional covariograms are demonstrated in figure 7. The same figures are obtainable for Lx1-transects.

In models *with nugget variance,* (7) must be modified into (9)

$$\text{sill}_{1xL} = \text{Cov}_{1xL}(0) + \frac{C_0}{L} = C \cdot \text{Corr}_{1xL}(0) + \frac{C_0}{L} = \text{partial sill}_{\text{point}} \cdot \overline{\text{Corr}}_{\text{Pin 1xL}} + \frac{\text{nugget}_{\text{point}}}{L} \qquad (9)$$

For $\text{Corr}_{1xL}(0)$, the relation (6) must be used in the exponential model. Again, because of the isotropy, (9) is valid for Lx1-transects, too.

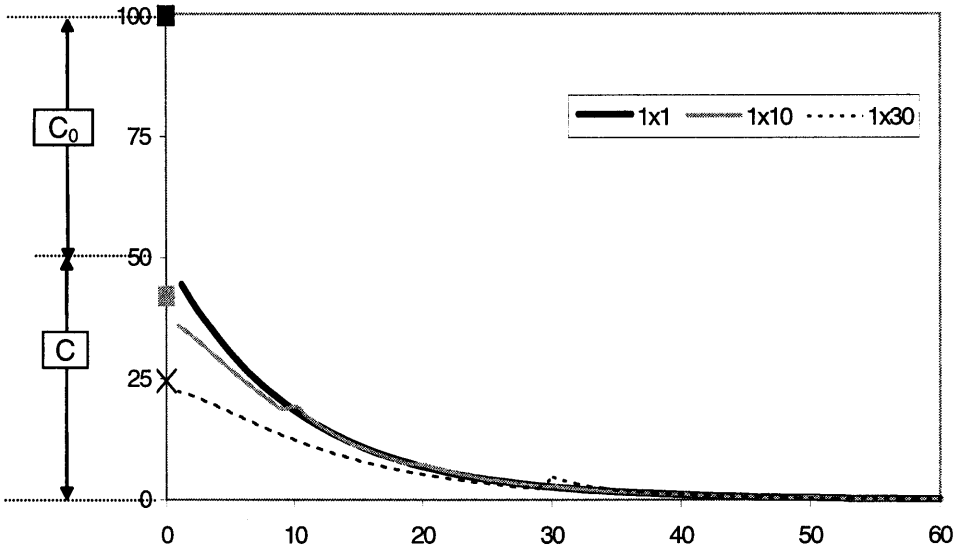

Fig. 7: Omnidirectional exponential covariograms for point data (1x1) and for transect data – simulation default: isotropic, A* = 10, C_0 = 50 and C = 50.

With increasing transect length L, the nugget part $\frac{C_0}{L}$ and $Cov_{1xL}(0)$ decrease, however, the PSS increases (figure 7). For $L \rightarrow \infty$, the *PSS* goes to $2C \cdot A^* / (2C \cdot A^* + C_0)$ (= 0.952 in the example). Here, the *PSS* increases from 0.5 for the point data over 0.88 for L = 10 and 0.932 for L = 30.

As in section 3.1, jump discontinuities are observable whenever h is an integral multiple of L. However, in contrast to the spherical model, this is valid for h without a limitation. In figure 7 the jumps are only observable for h = L.

Remark about the spherical model with nugget:
(9) is likewise valid for the spherical model with nugget. Here, $Cov_{1xL}(0)$ is given in (8), and for $L \rightarrow \infty$, the *PSS* goes to $3 \cdot C \cdot A / (3 \cdot C \cdot A + 4C_0)$.

3.3 Transects - default (3) – no nugget, anisotropy, exponential

When dealing with isotropic point data, the direction in which the transects are formed has no effect on the omnidirectional covariogram. Addionally, the directional covariograms for 1xL or Lx1 are exchangeable by changing the x- and y-direction. In the anisotropic case, however, there are considerable differences.

Therefore, at first we will highlight some differences to the introductory example in chapter 2. Be A_x^* the range parameter in x-direction and A_y^* in y-direction. Then, instead of (5), the correlation function for 1xL-transects in x-direction is

$$Corr_{1xL}^{x\text{-dir}}(h) = \frac{2}{L^2} \cdot \int_0^L (L-u) \cdot e^{-\sqrt{\left(\frac{h}{A_x^*}\right)^2 + \left(\frac{u}{A_y^*}\right)^2}} du$$

and for the y-direction, A* has to be replaced by A_y^* in (4).

For the Lx1-transects and for the y-direction, the function is

$$Corr_{Lx1}^{y\text{-dir}}(h) = \frac{2}{L^2} \cdot \int_0^L (L-u) \cdot e^{-\sqrt{\left(\frac{h}{A_y^*}\right)^2 + \left(\frac{u}{A_x^*}\right)^2}} du$$

and for the x-direction, A* has to be replaced by A_x^* in (4).

With (6), it follows that, unlike the isotropic case, $Corr_{1xL}(0) \neq Corr_{Lx1}(0)$.
If $A_x^* < A_y^*$, then $Corr_{1xL}(0) > Corr_{Lx1}(0)$, and vice versa.

For the defaults (3) from table 1 and transects 1x8 and 8x1, the covariograms are demonstrated in figure 8. Again, the directional covariograms are enveloping curves for the omnidirectional ones. It can be seen, that $Corr_{1x8}(0)$ is larger then $Corr_{8x1}(0)$, because A_x^* is smaller than A_y^*.

The anisotropy will be reinforced if the transects are oriented in the direction of the larger range parameter (A_y^*) (figure 8, a). In the other direction, the jumps are damped (figure 8, b). The maximum difference between the two directional correlograms is a function of A_x^*, A_y^* and L as well as of the direction of the transects. For $A_x^* = 1...15$, $L = 1...30$ and $A_y^* = const = 15$ the results are given in figure 9. In the above example, the maximum difference between the correlograms is 0.164 for 1x8, but only 0.116 for 8x1.

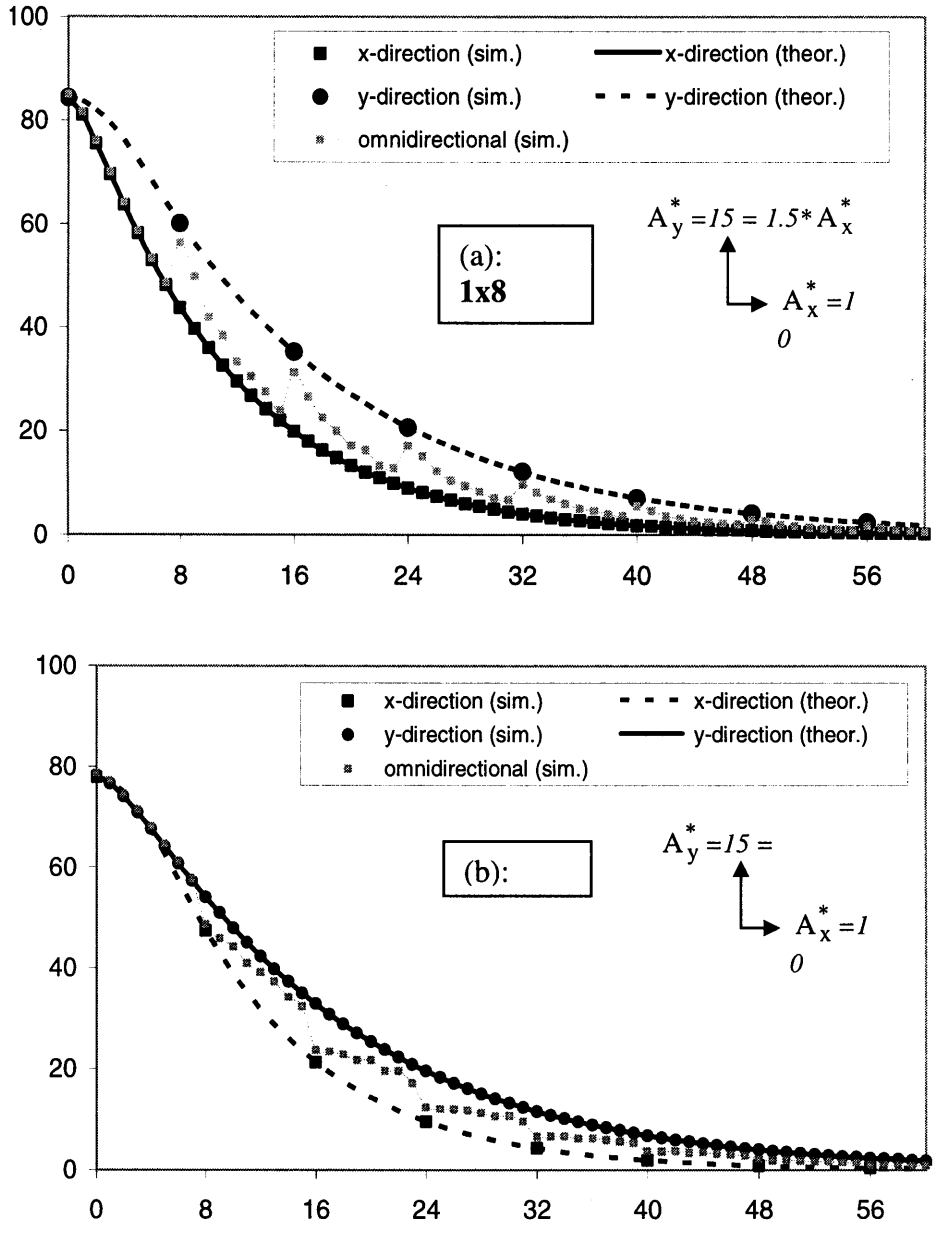

Fig. 8: Simulation default: anisotropic, $A^*_y = 15$, $A^*_x = 10$, $C_0 = 0$ and $C = 100$. Omnidirectional exponential covariograms for transect data with enveloping directional curves – (a) 1x8 and (b) 8x1.

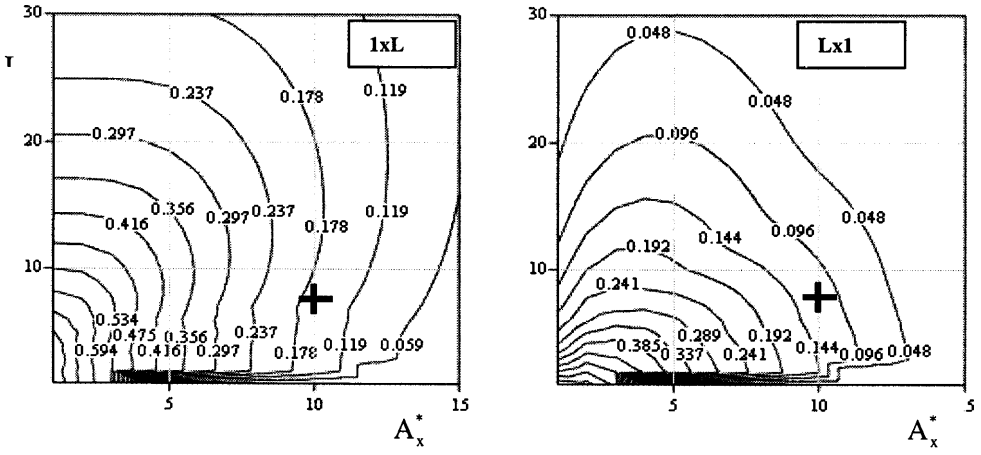

Fig. 9: Maximum differences between the two directional exponential regularized correlograms as a function of A_x^* and L, $A_y^* = 15$. + discussed example with $A_x^* = 10$ and L = 8.

3.4 Plots - default (1) – no nugget, isotropy, spherical

The above descriptions make plausible that similar results can be expected for plots. Because the graphs are very similar to those of transects we will refrain from presenting them here.
The reduction of the partial sill arises from the correlation within the plot. The larger the plot is, the smaller the partial sill and the nugget variance are:

$$\text{sill}_{axb} = \text{Cov}_{axb}(0) + \frac{C_0}{a \cdot b} = C \cdot \text{Corr}_{axb}(0) + \frac{C_0}{a \cdot b} = \text{partial sill}_{point} \cdot \overline{\text{Corr}}_{\text{P in plot}} + \frac{\text{nugget}_{point}}{a \cdot b}$$

In the case of isotropic point data, only quadratic plots provide the same sigmoid directional curves in both directions. In all other cases – isotropic point data and rectangular plots or anisotropic point data and quadratic/rectangular plots – regularization results in an anisotropy and in a model change compared to the model of the point data.

4. Summary of the simulation results and theoretical remarks

Independent of whether the point data follow the isotropic or anisotropic exponential or spherical model, the directional covariograms of the transect data show a sigmoid shape. For transects built up in y-direction, it is obvious that the shape in x-direction is sigmoid because many points lie in this direction. In y-direction, the values are the sparser the longer the non-overlapping transects become. For a real experiment, it follows that the uncertainty of an appropriate model choice is much higher in this direction. In principle, the same is true for plots. For the smaller side length, more points exist so that the sigmoid shape in this direction is much clearer than in the other.

For regularized data, it can be expected that an anisotropic model provides a better fit. If, nevertheless, an isotropic model will be fitted, a model error can a priori be expected. However, for isotropic point data, the maximal differences between the regularized directional covariograms of the transects are not very large. For the exponential model, the difference is at its maximum for $L \approx 1.8 \cdot A^*$ and equal to $C \cdot 0.068$. For the spherical model, it is at its maximum for $L \approx 0.82 \cdot A$ and equal to $C \cdot 0.122$. This is probably often not recognized in real experiments because other influences superimpose the effect of regularization.

If the point data are anisotropic and the larger range has the same direction as the transects (resp. the larger dimension of the plots), the anisotropy is more pronounced than if the transects were laid out in the other direction.

Whereas the changes of the nugget variance do not depend on the model of the point data, changes of the partial sill and range / range parameter do. Both the nugget variance and the partial sill decrease with an increasing length of transects or the area of plots. Although the quotient of spatial structure does not theoretically converge to 1, in real experiments one can expect that a model without nugget variance gives a sufficient proper fit with increasing transect length (plot size).

REFERENCES

Bartlett M. S. (1938). The Approximate Recovery of Information from Replicated Field Experiments with Large Blocks. Journal of Agricultural Science 28, 418-427.

Brownie, C.; Bowman, D.T.; Burton, J.W. (1993). Estimating spatial variation in analysis of data from yield trials: A comparison of methods. Agronomy Journal 85, 1244-1253.

Ersbøll A.K. (1996). Spatial Experimental Design. Proceedings III HARMA Meeting Cordoba, 112-125.

Fisher R.A. (1935). The Design of Experiments. Oliver and Boyd.

Journel A. G., Huijbregts Ch. J. (1978). Mining Geostatistics. Academic Press London.

Littell R.C., Miliken G.A., Stroup W.W., Wolfinger R.D. (1996). SAS System for mixed models. SAS Institute.

Papadakis J.S. (1937). Méthode statistique pour des expériences sur champ. Bull. Inst. Amél. Plantes à Salonique, No. 23.

Rendu J. M. (1981). An introduction to geostatistical methods of mineral evaluation. South African Institute of Mining and Metallurgy.

Schabenberger O., Pierce F.J. (2002). Contemporary statistical models for the plant and soil sciences. CRC Press.

Stroup W.W.; Baenziger P.S.; Mulitze D.K. (1994). Removing spatial variation from wheat yield trials: A comparison of methods. Crop Science 86, 62-66.

Stroup W.W. (2002). Power analysis based on spatial effects mixed – models: A tool for comparing design and analysis strategies in the presence of spatial variability. Journal of Agricultural, Biological, and Environmental Statistics 7 (4), 491-511.

Wiebe G. A. (1935). Variation and correlation in grain yield among 1,500 wheat nursery plots. Journal of Agricultural Research. 50, 331-357.

Yates F. (1938). The comparative advantages of systematic and randomized arrangements in the design of agricultural and biological experiments. Biometrika 30, 440-466.

Zimmerman D. L., Harville D. A. (1991). A random field approach to the analysis of field-plot experiments and other spatial experiments. Biometrics 47, 223 – 239.

Biometrical Letters
Vol. 44 (2007), No. 2, 165-166

CORRIGENDUM

Christel Richter, Bärbel Kroschewski

Some considerations on the use of geostatistical methods in agricultural field trials. Part I. From point to regularized data – theoretical considerations

The corrected Figure 1 (page 53) and Figure 8 (page 63) are shown below.

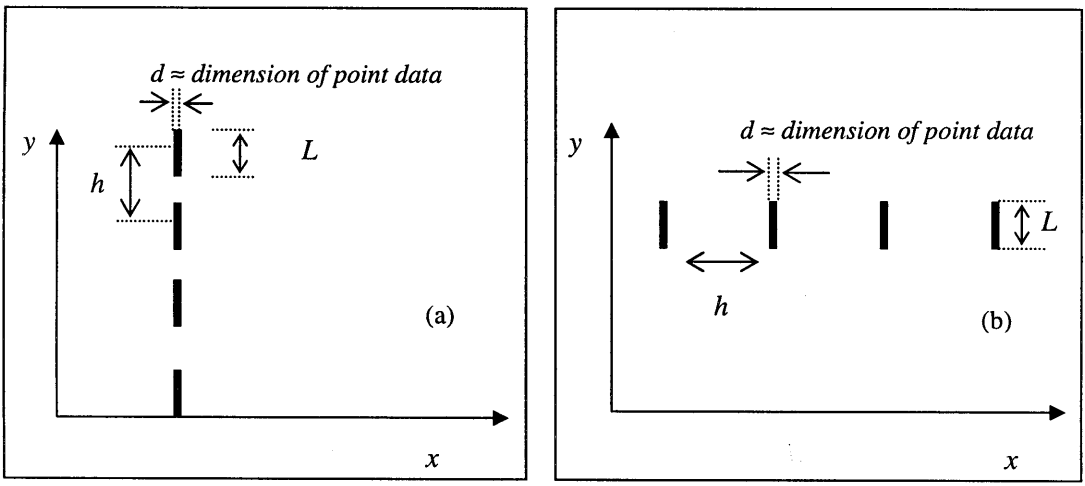

Fig. 1: Two forms of one-dimensional regularization in xy-plane: regularization by samples within a core (a) and regularization over constant thickness (b).

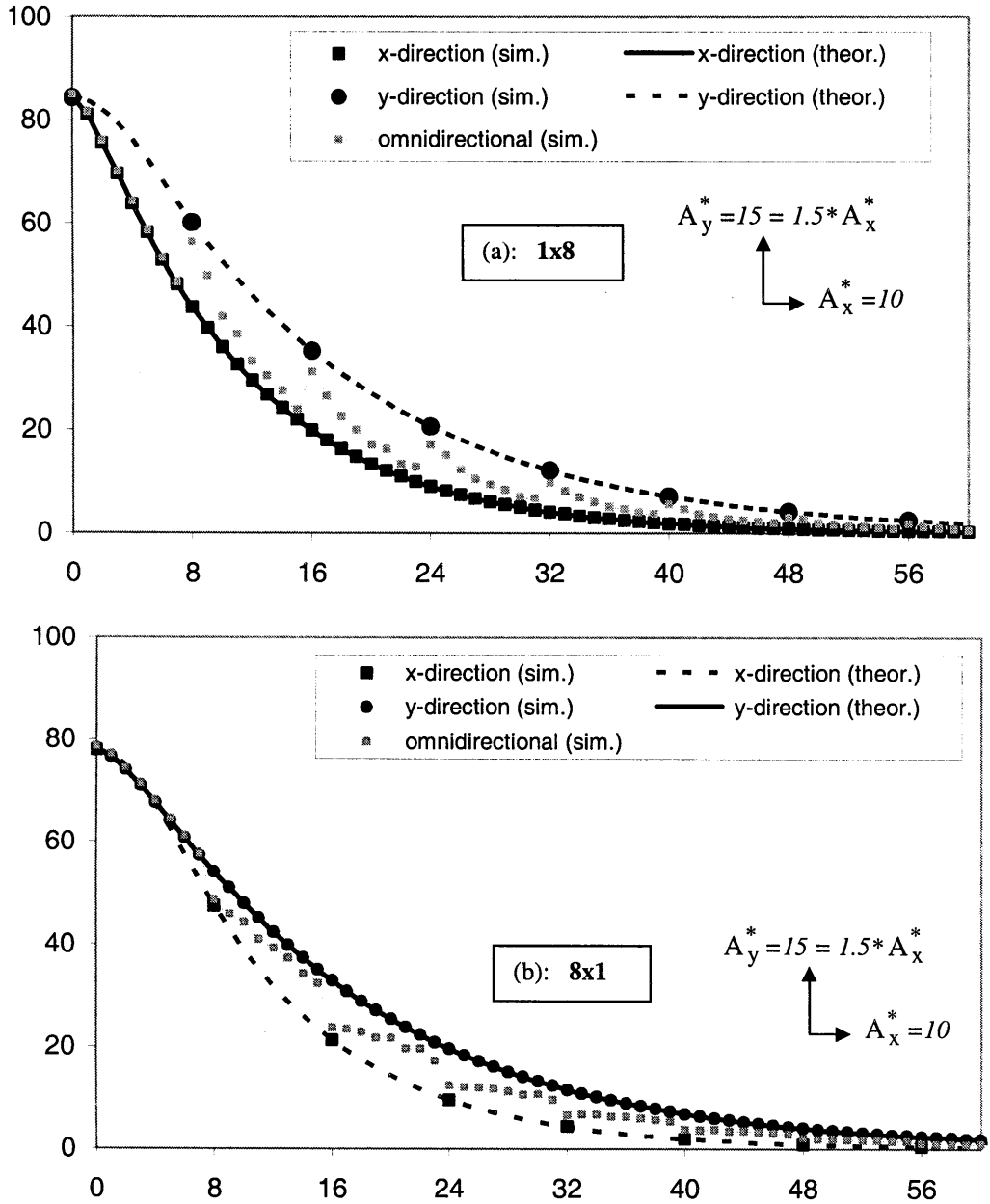

Fig. 8: Simulation default: anisotropic, $A^*_y = 15$, $A^*_x = 10$, $C_0 = 0$ and $C = 100$.

Omnidirectional exponential covariograms for transect data with enveloping directional curves – (a) 1x8 and (b) 8x1.